

Electrochimica Acta

Elsevier Editorial System(tm) for

Manuscript Draft

Manuscript Number: CAP19-01R2

Title: Achieving on Chip Micro-Supercapacitors Based on CrN Deposited by Bipolar Magnetron Sputtering at Glancing Angle

Article Type: VSI: ISEECap 2019 Nantes

Keywords: Transition metal nitrides; Electrochemical capacitors; GLAD; On chip Micro-supercapacitor

Corresponding Author: Dr. Emile HAYE,

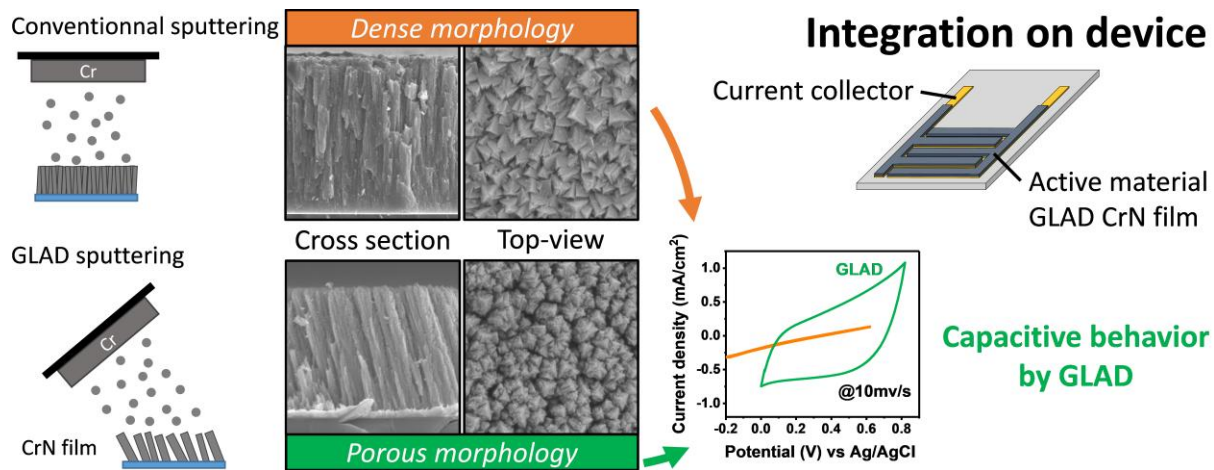
Corresponding Author's Institution: UNamur

First Author: Emile HAYE

Order of Authors: Emile HAYE; Amine ACHOUR; Abdelouadoud GUERRA; Fatsah MOULAI; Toufik HADJERSI; Rabah BOUKHERROUB; Adriano PANEPINTO; Thierry BROUSSE; Jean-Jacques PIREAUX; Stéphane LUCAS

Manuscript Region of Origin: BELGIUM

Abstract: The enhancement of the surface area and ordering of mesopores is a key parameter to increase the specific capacitance of electrochemical capacitors (ECs). These parameters can improve the electrolyte accessibility to the active material in order to improve its charge storage. In this work, magnetron sputtering at glancing angle (GLAD) is used in order to enhance the porosity of CrN for use as electrode material in ECs. The GLAD technique consists on tilting the substrate according to the deposition flux allowing the formation of well-separated columns due to a ballistic shadowing effect. Four different tilts of 0°, 45°, 60° and 75° were explored. While the CrN films deposited at 0° or 75° do not show any capacitive behaviour, a high areal capacitance is obtained at 45° or 60° (35.4 mF.cm⁻² at a current density of 1.2 mA.cm⁻² in 0.5M H₂SO₄ electrolyte) with a good cycling stability over 10000 cycles. On chip interdigitated micro-supercapacitors (MSCs) were assembled with a maximum energy density of 2 μWh.cm⁻² (15.3 mWh.cm⁻³) at a power density of 20 μW.cm⁻² (0.15 W.cm⁻³). The GLAD strategy can be generalised to other materials deposited by physical vapour deposition techniques, for highly porous electrodes, with improved electrochemical energy storage properties.





03.09.2019

To S. Trasatti
Editor-in-Chief
Journal of Power Sources
Elsevier

Dear S. Trasatti,

Please find enclosed our revised manuscript entitled "Achieving on Chip Micro-Supercapacitors Based on CrN Deposited by Bipolar Magnetron Sputtering at Glancing Angle" by Haye *et al*, which I am submitting on the behalf of the co-authors, for publication in ***Electrochimica Acta***. Please note that this manuscript is not under consideration and will not be submitted elsewhere, before your final decision. ***Electrochimica Acta*** is an important resource for our research and we are pleased to have quite a few publications in this journal over the past few years.

We revised our manuscript to address the comments made by the Editorial Office and the 1st reviewer. This revised version is based on new samples and new measurements, as requested by the reviewer.

Your feedback and input on the quality of the manuscript is highly appreciated. We hope that the revised manuscript will now be accepted for publication in your Journal. We, however, assure you that, if required, any changes suggested to further improve the quality of this research article will be duly made.

Thanking you in advance.

With best regards.

On the behalf of co-authors

Dr. Amine ACHOUR

Dr. Emile HAYE

Laboratoire Interdisciplinaire de Spectroscopie Electronique (LISE)

Namur Institute of Structured Matter (NISM)

University of Namur, Belgium

Suggested Referees:

1. Aurélien BESNARD,
Expert in GLAD deposition
aurelien.BESNARD@ensam.eu
LaBoMaP
Ecole Nationale Supérieure d'Arts et Métiers
Rue porte de Paris, 71250 Cluny – France

2. Nicolas MARTIN
nicolas.martin@femto-st.fr
Expert in GLAD deposition of thin film, expert in PVD coating
FEMTO-ST
15B avenue des Montboucons
25030 Besançon cedex – France

3. Christophe LETHIEN
christophe.lethien@iemn.univ-lille1.fr
Expert in nitride materials for supercaps application
IEMN, Université de Lille 1 Sciences et Technologies,
BP 60069, 59652 Villeneuve d'Ascq cedex – France

Manuscript ID: Ref. No.: CAP19-01R1

Title: Achieving High Performance on Chip Micro-Supercapacitors Based on CrN Deposited by Bipolar Magnetron Sputtering at Glancing Angle

Electrochimica Acta

Authors: Haya. *et al.*

Thanks to the reviewers.

The manuscript has been revised according to the reviewer comments, based on new measurement on new samples. We have now additional material characterization (RBS, AFM, and resistivity) on similar samples. These new results were originally for another study, we thus only disclose critical information for the current work.

Reviewer #1:

I am disappointed with the authors' responses. Many of my comments are in fact easy to address but unfortunately, the authors seem refuse to make any additional measurements.

I therefore do not recommend the publication of this manuscript.

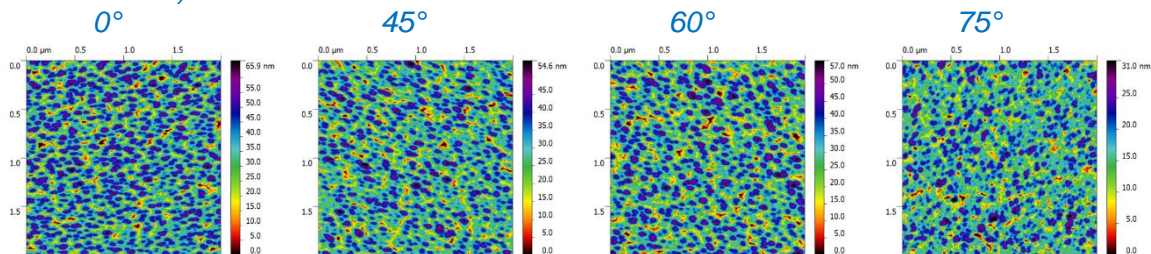
Authors' response:

Parallel to the current work, we performed new deposition of CrN coating in GLAD configuration (for another work), at different deposition angle, in similar configuration than the current work. We carried out further characterization on sample similar the ones used for the present work (0, 45, 60, 75°). So, we have now additional material characterization (RBS, AFM, resistivity) on similar samples. These new results are for a new paper, so we only disclose critical information for the current work.

1. Q1. SEM surely is not "the only possible way to estimate the surface area". People have been using AFM and ellipsometry to determine the surface area/porosity of nitride thin films.

Authors' response:

Yes, the reviewer is right, other methods are possible, but they are not really suitable in our case: we performed AFM measurements (see map below), but the size of the AFM tip is not representative of the electrolyte access to the active material. We only obtain the top surface area (and deep hole between columns are not taken into account). From AFM measurements (at least, in our setup), we obtained heights of 30-60nm, and a roughness (Ra) of 9.5, 7.6, 8.1 and 5.5 nm for 0, 45, 60 and 75°. These results are not in agreement with SEM measurements (we can see holes of 100-500nm).



Concerning ellipsometry, the porosity can be determined, but not the surface area, to the best of our knowledge. For the same porosity, the surface area can be drastically different.

	<p><i>Moreover, ellipsometry takes into account closed pores, which is not representative of the electrolyte access.</i></p> <p><i>The best method to determine the surface area would be based on adsorption method (BET, or ellipsometry combined with water adsorption), but we don't have access to it, and the measurement on coating required large sample (to get accurate measurement).</i></p> <p><i>In the present case, we are much more confident in SEM images and their direct observation, with qualitative observation, than AFM measurements.</i></p> <p><i>We are still open to discuss this point if the reviewer disagree with our point of view.</i></p>
2.	<p>Q2. If the authors did not measure the resistivity of their films, how do they know that "the resistivity was similar to other reported work on CrN"?</p>
	<p><i>Authors' response:</i></p> <p><i>We have measured the resistivity of our coating, the values were not given in the previous version of the manuscript.</i></p> <p><i>We also measured the resistivity of the second set of sample, very close to the first one, with values of 5.5×10^{-2}, 1.2×10^{-1}, 2.0×10^{-2} and $6.9 \times 10^{-2} \Omega \cdot \text{cm}$ for 0, 45, 60 and 75° orientation. The value are in agreement with the literature (ρ ranges from 3×10^{-4} to $20 \Omega \cdot \text{cm}$, see DOI: 10.1103/PhysRevB.83.165205 and DOI: 10.1103/PhysRevB.82.045116).</i></p> <p><i>The increase of ρ with the deposition angle is due to the higher oxygen incorporation in the coating (the deposition rate decreases, but the content of residual oxygen in the chamber remains constant, so it increases in the coating).</i></p>
3.	<p>Q3. I understand that areal capacitance is more important in microdevices and that is why I only asked the authors to provide the mass loading in 3-electrode measurements. In this way, the readers can better understand how the intrinsic performance of the CrN in this work compares to other reported CrN. The mass loading can be roughly estimated by weighting the substrate before and after deposition, which should be not that difficult or "impossible".</p>
	<p><i>Authors' response:</i></p> <p><i>The mass loading determined by weighing the sample before and after deposition is not accurate at all for such coating thickness (it works if we use a sample with very large surface).</i></p> <p><i>Quartz balance measurement during deposition is good, but still suffers from two major problems:</i></p> <ol style="list-style-type: none"> <i>(1) It assumes a bulk density of chromium nitride, and the coating is porous, so the mass loading is overestimated.</i> <i>(2) The setup of the quartz balance is good for measurement in front of the target, or slightly tilted. At higher angle, our device is not really adapted (the device starts to obstruct the flux of species).</i> <p><i>As alternative, RBS (Rutherford Backscattering Spectroscopy) measurement have been performed on similar sample, and the density of the coating can be determined, with good accuracy, combining RBS and thickness measurement (check the supplementary information of Hays et al. DOI: 10.1016/j.surfcoat.2018.07.009).</i></p> <p><i>Knowing the density and the surface of the coating, we can estimate the mass loading of active material. The density of such coating is around $4.5 \text{ g} \cdot \text{cm}^{-3}$ (lower than bulk CrN, due to the presence of contaminant such as oxygen, that decrease the measured RBS density).</i></p> <p><i>Considering the volume of deposited coating, it gives a mass of $\approx 2 \times 10^{-5} \text{ g}$ for the MSC device.</i></p>

	<i>The information is now provided.</i>
4.	Q4. To be honest, I was surprised by this response. What is the temperature difference? How many samples have the authors tested? Are they showing constant results?
	<i>Authors' response:</i> <i>The measurement has been done in two steps, the break is due to the ON/OFF/ON of the setup. Two samples have been tested with similar results.</i>
5.	Q5. I have no idea why the authors showed me the calculation process. My concern is that the calculation that the authors used obviously overestimates the real capacitance. The slope method should be used only if the materials show capacitive properties (ideally rectangular-shaped CV curves and triangular-shaped CD curves, normally seen for carbons). The integrate method is a more appropriate way to determine the capacitance of CrN in this case, as the it has both contributions from capacitive and Faradaic reactions (the CD curve is nonlinear, and not symmetric neither).
	<i>Authors' response :</i> <i>Concerning the capacitance method calculation: The slope method was used when we study the influence of the current densities of the charge-discharge curves on the specific capacitance and the integration method (based on cyclic voltammograms CV area) when we study the influence scan rates on the specific capacitance.</i> <i>This method has been applied in numerous work (see ref below).</i> <i>B S Singu 2016 - J Solid State Electrochem DOI 10.1007/s10008-016-3309-1</i> <i>B S Singu 2016 - Ionics DOI 10.1007/s11581-016-1669-2</i> <i>P P Sahay 2017 - J Solid State Electrochem DOI 10.1007/s10008-017-3574-7</i> <i>B S Singu 2016 - J Solid State Electrochem DOI 10.1007/s10008-017-3661-9</i> <i>To avoid confusion, the following sentence has been added in the revised manuscript: " It is noteworthy to mention that the capacitance values versus current density given in this work can be overestimated. This is because we used the slop method to estimate the capacitance versus the current densities, while this method is accurate only for ideally rectangular-shaped CV curves and triangular-shaped CD curves and which is not the case for our electrodes".page 19</i>
6.	Q6. The authors did not test the CrN-45 for devices and how can they conclude that "the volumetric capacitance of CrN-60 is close to that of CrN-45"?
	<i>Authors' response:</i> <i>Yes, we did not test the CrN 45 for device, as it is mentioned in the manuscript. However, we determined the volumetric capacitance on silicon sample, with similar values of 454.5 and 389.9 F.cm⁻³ for CrN45 and CrN60 sample.</i>
Reviewer #2: The authors have addressed all the necessary comments as advised by the referee. Hence I would like to recommend it for publication in Electrochimica Acta in the current form.	
1.	<i>Authors' response:</i> <i>Thank for the review of our work.</i>

Reviewer #3:

The authors have improved the manuscript considering most of the reviewer comments. They only have to check some English mistakes. To my opinion, the manuscript can be now accepted for publication.

Authors' response:

Thank for the review of our work. The mistakes have been corrected.

Achieving on Chip Micro-Supercapacitors Based on CrN

Deposited by Bipolar Magnetron Sputtering at Glancing Angle

Emile HAYE^{1,*}, Amine ACHOUR^{1,*}, Abdelouadoud GUERRA^{2,3,4}, Fatsah MOULAI²,
Toufik HADJERSI², Rabah BOUKHERROUB³, Adriano PANEPINTO⁵, Thierry
BROUSSE^{6,7}, Jean-Jacques PIREAUX¹, Stephane LUCAS⁸

¹ *Laboratoire Interdisciplinaire de Spectroscopie Electronique (LISE), Namur Institute of Structured Matter (NISM), University of Namur, 61 Rue de Bruxelles, 5000 Namur, Belgium.*

² *Centre de Recherche en Technologie des Semi-conducteurs pour L'Energétique (CRTSE), Division TESE, 2 Bd. Frantz Fanon, B.P. 140 Alger-7 Merveilles, Alger, Algeria.*

³ *Univ. Lille, CNRS, Central Lille, ISEN, Univ. Valenciennes, UMR 8520, IEMN, F-59000 Lille, France*

⁴ *Université Ferhat Abbas Sétif 1, El Bez, Sétif 19000, Algérie*

⁵ *Chimie des Interactions Plasma-Surface (ChIPS), Université de Mons, 23 Place du Parc, 7000 Mons, Belgium.*

⁶ *Institut des Matériaux Jean Rouxel (IMN), Université de Nantes, CNRS, 2 rue de la Houssinière, BP32229, 44322, Nantes Cedex 3, France*

⁷ *Réseau sur le Stockage Electrochimique de l'Energie (RS2E), FR CNRS, 3459, France*

⁸ *Laboratoire d'Analyse par Réactions Nucléaires (LARN), Namur Institute of Structured Matter (NISM), University of Namur, 61 Rue de Bruxelles, 5000 Namur, Belgium.*

* Corresponding author:

Dr. Amine ACHOUR: amine.achour@unamur.be and a_aminph@yahoo.fr

Dr. Emile HAYE: emile.haye@unamur.be

Highlights

- The apparent porosity of sputtered CrN films was improved by GLAD deposition
- A maximum specific capacitance of 35.4 mF cm^{-2} was achieved at 1.2 mA cm^{-2}
- On chip micro-supercapacitor (MSC) based on sputtered porous CrN material is fabricated
- The CrN-based MSC exhibited both high energy and power densities

1
2
3
4
5
6
7
8
9
10
11
12
13
14
15
16
17
18
19
20
21
22
23
24
25
26
27
28
29
30
31
32
33
34
35
36
37
38
39
40
41
42
43
44
45
46
47
48
49
50
51
52
53
54
55
56
57
58
59
60
61
62
63
64
65

Abstract

The enhancement of the surface area and ordering of mesopores is a key parameter to increase the specific capacitance of electrochemical capacitors (ECs). These parameters can improve the electrolyte accessibility to the active material in order to improve its charge storage. In this work, magnetron sputtering at glancing angle (GLAD) is used in order to enhance the porosity of CrN for use as electrode material in ECs. The GLAD technique consists on tilting the substrate according to the deposition flux allowing the formation of well-separated columns due to a ballistic shadowing effect. Four different tilts of 0°, 45°, 60° and 75° were explored. While the CrN films deposited at 0° or 75° do not show any capacitive behaviour, a high areal capacitance is obtained at 45° or 60° (35.4 mF.cm⁻² at a current density of 1.2 mA.cm⁻² in 0.5M H₂SO₄ electrolyte) with a good cycling stability over 10000 cycles. On chip interdigitated micro-supercapacitors (MSCs) were assembled with a maximum energy density of 2 μWh.cm⁻² (15.3 mWh.cm⁻³) at a power density of 20 μW.cm⁻² (0.15 W.cm⁻³). The GLAD strategy can be generalised to other materials deposited by physical vapour deposition techniques, for highly porous electrodes, with improved electrochemical energy storage properties.

Keywords: Transition metal nitrides; Electrochemical capacitors; GLAD; On chip Micro-supercapacitor

1. Introduction

Physical vapour deposition (PVD) techniques are widely used for material synthesis, in the form of films, for different applications including semiconductor technology, medical devices, smart coatings, or cutting tools [1–4]. Recently, there has been an impressive research effort toward the fabrication of electrodes deposited by PVD for energy storage devices such as Li-ions/micro-batteries [5,6] or electrochemical capacitors (ECs)/micro-supercapacitors (MSCs) [7–9]. In particular, in the case of ECs electrodes, the PVD techniques offer the alternative solution to most of the problems faced during processing of powder into packed films [6,8,9]. These problems consist of bad adhesion to the current collector, loss of accessible volume to the electrolyte and incompatibility with standard micro-fabrication protocols. Indeed, PVD can produce films with good adhesion, controlled thickness, composition and morphology [1–4,6,9,10]. Thus, using PVD to fabricate electrodes for ECs, and especially for micro-supercapacitors, would be an interesting alternative solution to most of the problems encountered during processing of powder into packed films.

Metal oxides including RuO_2 [11], MnO_2 [12] and transition metal nitrides such as TiN [13,14], VN [15], TiVN [16], RuN [17] and CrN [18,19], have been deposited by PVD methods for use as electrodes in ECs. In addition, the deposition parameters were also adjusted, in order to increase the porosity of the films, and thus, enhance their specific capacitance. For instance, nitrogen flux has been controlled in the case of TiN electrodes [13], while the pressure and deposition temperature have been adjusted in the case of VN [20] and CrN [18] electrodes in order to produce porous films with enhanced electrochemical energy storage. In this work, we used bipolar magnetron sputtering at glancing angle (GLAD)

1 as a new strategy, in the field of ECs, to improve the apparent porosity of CrN films. The
2 GLAD strategy simply entails substrate tilting with respect to the target during film
3 deposition. The GLAD method allows to modify the morphology of the deposited coating,
4 from dense to porous, and the formation of inclined columns. Such features have found
5 applications in optical devices (polarized light emitters), sensors devices (humidity sensors)
6 or energy devices (solar energy conversion) [21–23]. Herein, four different tilt angles of 0,
7 45, 60 and 75° were explored. The areal capacitance value of the resulting CrN electrodes can
8 reach capacitance values as high as 35.4 mF.cm⁻² at a current density of 1.2 mA.cm⁻², with a
9 stable cycle life exceeding 10,000 cycles. Moreover, the apparent porosity of the CrN
10 electrode can be controlled by tailoring the deposition angle inside the chamber during film
11 growth, which affects both the areal capacitance and power density of the electrodes. In
12 contrast to the method used in Ref [19] involving selective etching of Cu from CrCuN film in
13 order to obtain porous CrN films, our method is simple and consists in a single step process.
14 In addition, it is scalable and can be easily generalized for other types of materials deposited
15 by PVD techniques in order to obtain high porous electrodes for energy storage applications.
16
17
18
19
20
21
22
23
24
25
26
27
28
29
30
31
32
33
34
35
36
37
38
39

40 2. Experimental methods

41 2.1. Synthesis of CrN films

42 The CrN thin films have been synthesized by combining magnetron sputtering and glancing
43 angle deposition (GLAD) in a 1m³ semi-industrial hexagonal chamber from D&M
44 Vacuumsystemen [2]. Two planar chromium targets (7.5 × 35 cm, 99.99% purity, from
45 Neyco) have been sputtered in an argon and nitrogen gas mixture, at respectively 150 and 120
46 sccm, with gas injected at the targets surface. The pressure was set at 5 mTorr (0.66 Pa) and
47 continuously adjusted with a throttle valve. The targets are sputtered in bipolar mode, using a
48
49
50
51
52
53
54
55
56
57
58
59
60
61
62
63
64
65

1
2
3
4
5
6
7
8
9
10
11
12
13
14
15
16
17
18
19
20
21
22
23
24
25
26
27
28
29
30
31
32
33
34
35
36
37
38
39
40
41
42
43
44
45
46
47
48
49
50
51
52
53
54
55
56
57
58
59
60
61
62
63
64
65

Magpuls QP-1000/20 10 kW pulse unit, at a mean current of 2 A, a duty cycle of 50% and a frequency of 2500 Hz. Silicon substrates were static and mounted in front of one cathode, with tilted substrate holder at 0, 45, 60 and 75°. Prior to the deposition of CrN film, an interface layer of Ti and Au with thickness of 80 nm is deposited. The Ti/Au layers were chosen as substrates for CrN deposition, because the device is made of gold as current collector deposited on Ti buffer layer (as explained in the supporting information). The role of the Ti buffer is the improvement of the gold adhesion on silicon. Therefore, in order to make an honest comparison between CrN film tested in the three electrode configurations and the CrN deposited on the device (made of gold current collector) we have chosen Ti/Si as a buffer in the case of CrN film in order to exclude any effect of the substrate concerning the resistivity and CV shapes.

2.2. Sample characterization

2.2.1 Structural and surface characterization

The top and cross section morphologies of the samples have been investigated using scanning electron microscopy (SEM) using a JEOL JSM 7500F microscope. The thickness of the samples has been measured both by cross-section observation in SEM and using a stylus profilometer (Bruker Dektak), both measurements being in good agreement. The structural characterization of the samples was performed by X-ray diffraction (XRD) using a PANalytical Empyrean diffractometer working with the Cu K α radiation ($\lambda = 0.1546$ nm) in the grazing incidence configuration (GA = 0.5°). The X-ray source voltage was fixed at 45 kV and the current at 40 mA. For surface chemical analysis, XPS measurements were carried out on a Thermo Scientific K-Alpha spectrometer using a monochromatic Al K α radiation (1486.68 eV) with a spot size of 250×250 μm . A flood gun was used for charge compensation

1 and the C1s line at 284.8 eV was used as a reference to correct the binding energies for
2 charge energy shift. The resistivity of the film has been determined by four point probes
3
4
5 measurements.
6
7
8
9

10 **2.2.2. Electrochemical characterization**

11
12 Electrochemical studies of the CrN electrodes were carried out using a
13
14 potentiostat/galvanostat Metrohm-Autolab PGSTAT128N at room temperature in a typical
15
16 three-electrode electrochemical cell. The cell is composed of two parts assembled face to
17
18 face. The lower part has a copper current collector and the upper part is made of Teflon and
19
20 filled with the electrolyte. It also has a hole at the bottom to enable the contact between the
21
22 electrode and the electrolyte. The CrN sample was used as working electrode, Ag/AgCl as
23
24 reference electrode and Pt foil as counter electrode. In this cell, only the side coated with CrN
25
26 was in contact with the electrolyte ($S = 0.5 \text{ cm}^2$). The other side of the samples was contacted
27
28 with the copper current collector by using silver paste to ensure a good electrical contact.
29
30
31
32
33
34
35

36 Interdigitated CrN/CrN micro-supercapacitors were evaluated by connecting each electrode
37
38 to the galvanostat/potentiostat while wetting the device with the H_2SO_4 electrolyte.
39
40
41

42 The electrodes were characterized by cyclic voltammetry (CV) and Galvanostatic Charge-
43
44 Discharge (GCD) in H_2SO_4 (0.5 M) aqueous solution. The charge transfer and ion diffusion
45
46 properties study of the CrN thin film electrodes were conducted by electrochemical
47
48 impedance spectroscopy (EIS) measurements. The EIS measurements were carried out in the
49
50 frequency range of 100 kHz–10 mHz by plotting spectra using 10 points per frequency
51
52 decade at open circuit potential (OCP) in 0.5 M H_2SO_4 electrolyte at room temperature. The
53
54 capacitance calculation details according to Ref [22,23] are given in the supplementary
55
56 information.
57
58
59
60
61
62
63
64
65

1 In the present work, only areal and volumetric capacitance of the CrN deposits and the
2 corresponding micro-devices are provided. It should be noted that the mass of the device has
3 not a meaning because the most important is the area that is occupied by the device and not
4 its mass [8].
5
6
7
8
9

10 11 12 13 14 **3. Results and discussion** 15

16 17 **3.1. Evaluation of CrN electrodes deposited at different angles** 18 19

20 21 **3.1.1. Structural and surface characterization** 22

23 Figure 1 shows the cross section and top view SEM images of the CrN films deposited at
24 different glancing incidence. All the samples exhibit a dense columnar structure, a typical
25 morphology obtained under similar conditions [2,24], with small cubic crystallites growing
26 normal to the surface. The tilting of the sample (defined by α , see supplementary information
27 and Figure S1 for the geometrical considerations) leads to a (i) change of the morphology, (ii)
28 a decrease of the thickness, from 1870 nm at 0° down to 1210 nm at 75° of incidence, and
29 (iii) a global increase of the tilting angle of the columns β . The increase of β is observed up to
30 $\alpha = 60^\circ$, while the columns are slightly less tilted than for $\alpha = 60^\circ$. Moreover, we observe a
31 large difference between experimental β angles and those from predictive models (see Figure
32 S2), even at low α angle. This evolution has already been reported by Besnard et al. [21],
33 where a saturation of tilting angle occurs, and a discrepancy with the predictive model (see
34 supplementary information). It is worth to mention that in our case, the nanostructures are
35 deposited on silicon substrates, which means that material quantity available is very low, and
36 therefore, in contrast to powder, the Brunauer-Emmett-Teller (BET) analysis is not really
37 suitable. The determination of the real surface area is difficult in this case, because of the
38 small spaces between columns. AFM measurements have been performed, but are not
39
40
41
42
43
44
45
46
47
48
49
50
51
52
53
54
55
56
57
58
59
60
61
62
63
64
65

representative of the real surface that is accessible to the electrolyte (only the top surface area can be determined, due to the tip size), and are not presented.

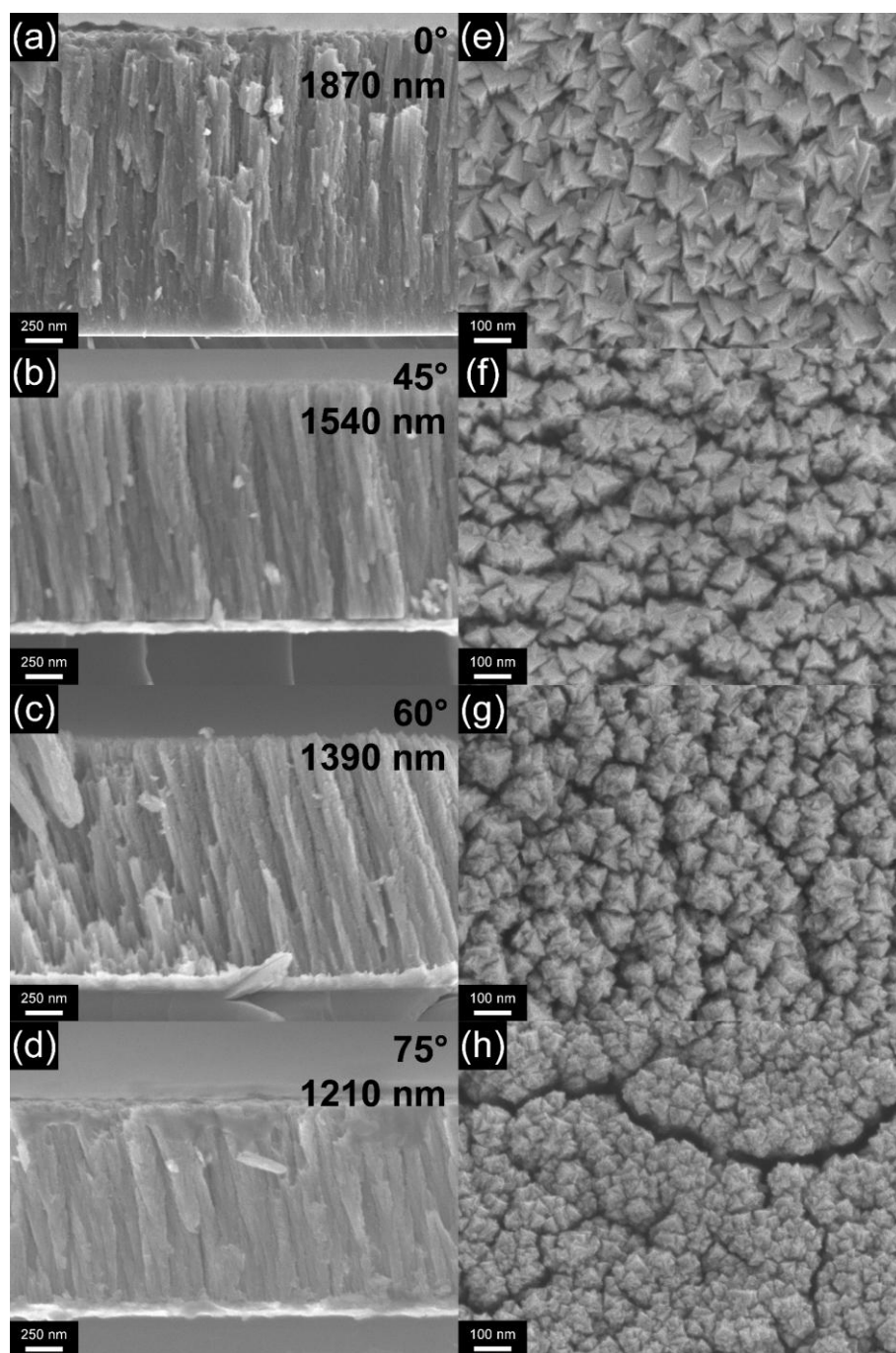


Fig.1. Top view SEM images of CrN films (a) CrN0° (b) CrN45°, (c) CrN60° and (d) CrN75°. Cross section SEM images of CrN films (e) CrN0° (f) CrN45°, (g) CrN60° and (h) CrN75°.

1 The influence of the tilting angle is attributed to the use of non-punctual source: the presence
2 of the racetrack modifies the ballistic regime of the sputtered species, and deposition of
3 matter with non-ballistic regime, due to collision, occurs. It results in columns that are less
4 tilted compared to thermal evaporation process or very low pressure deposition. Moreover,
5 the use of dual bipolar magnetron sputtering (with two targets) has a drastic influence on the
6 spatial and energy distribution of the species, increasing the non-ballistic regime contribution,
7 and thus decreasing the column tilt angle β even though the substrate holder is set in front of
8 one cathode. These mechanisms are beyond the scope of the paper, and will be further
9 investigated in a forthcoming paper.

10 Overall, the increase of tilt angle results in a more porous structure: at 0° , the structure is
11 denser, without voids between columns (Figure 1a & e), and cubic crystallites of ≈ 100 nm are
12 observed on the top surface. Both CrN 45° and CrN 60° exhibit similar morphology, but a
13 different tilting angle (respectively $10.8 \pm 0.8^\circ$ and $16.4 \pm 0.7^\circ$), with smaller cubic
14 crystallites, about 50-100 nm (Figure 1f & g), and more open voids between the top of the
15 columns. The increase of the incidence up to 75° does not significantly affects the shape of
16 the columns. However, it drastically reduces the crystallites size (< 50 nm) which merge
17 together to close open porosity as can be observed on the top surface from Figure 1h. The
18 same evolution has recently been reported for TiN thin films [22]. Thus, even if the voids
19 between columns are very similar for samples CrN 45° , CrN 60° and CrN 75° , the accessible
20 porosity will be drastically decreased for this last sample due to the close packed array of
21 nanocrystallites emerging on the top surface, unlike the two other samples which still exhibit
22 open porosity from SEM top views. These changes are attributed to the shadowing effect,
23 which is more intense using a higher incidence [25,26]. The presence of the growing columns
24 stops the line-of-sight flux of arriving species, creating shadow area that modifies the growth
25 mechanism. It results in a lower mobility of adatoms and lower crystallite size, in addition to
26
27
28
29
30
31
32
33
34
35
36
37
38
39
40
41
42
43
44
45
46
47
48
49
50
51
52
53
54
55
56
57
58
59
60
61
62
63
64
65

1 the creation of voids between columns [27,28]. It is worth mentioning that the difference of
2 grain size as well as the separation of columns by voids and defects in each case can deeply
3 influence both the electrical and electrochemical performance (inter-columnar porosity)
4 behaviour of CrN electrodes deposited at different tilt angles. Finally, the voids between
5 columns, estimated from SEM observations, are less than 20 nm, suggesting the presence of a
6 mesoporous network CrN_{45°} and CrN_{60°} samples. Due to the low amount of active material
7 and to the limited surface of thin film samples, it was not possible to further estimate the
8 pores size distribution by gas adsorption techniques.
9

10 In addition to the top view SEM images of CrN films, the cubic structure is also confirmed by
11 GA-XRD measurements (Figure 2a), with diffraction peaks at 37.5°, 43.6°, 63.4° and 76.0°
12 attributed to (111), (200), (220) and (311) planes, respectively. All the diffraction peaks have
13 a significant increase of the full width at half maximum (FWHM) as the deposition angle
14 increases. The FWHM of (111) diffraction peak has been used to estimate the grain size using
15 the Scherrer formula; the grain size decreases from 18 to 9 nm as the deposition angle
16 increases from 0 to 75°, in good agreement with the SEM observation. Due to the tilted
17 columnar morphology and the use of GA-XRD, the intensity ratio strongly depends on the
18 measurement method and the sample position during the measurement. Thus, the comparison
19 of intensity is not really convenient. However, a shift of the diffraction peaks is clearly
20 observed as the deposition angle increases. This effect is attributed to increase of the oxygen
21 content at high angles, due to the lower deposition rate. The presence of oxygen in metal
22 nitride thin film is frequently reported [29,30], and its content decreases as the deposition rate
23 increases.
24
25
26
27
28
29
30
31
32
33
34
35
36
37
38
39
40
41
42
43
44
45
46
47
48
49
50
51
52
53
54
55
56
57
58
59
60
61
62
63
64
65

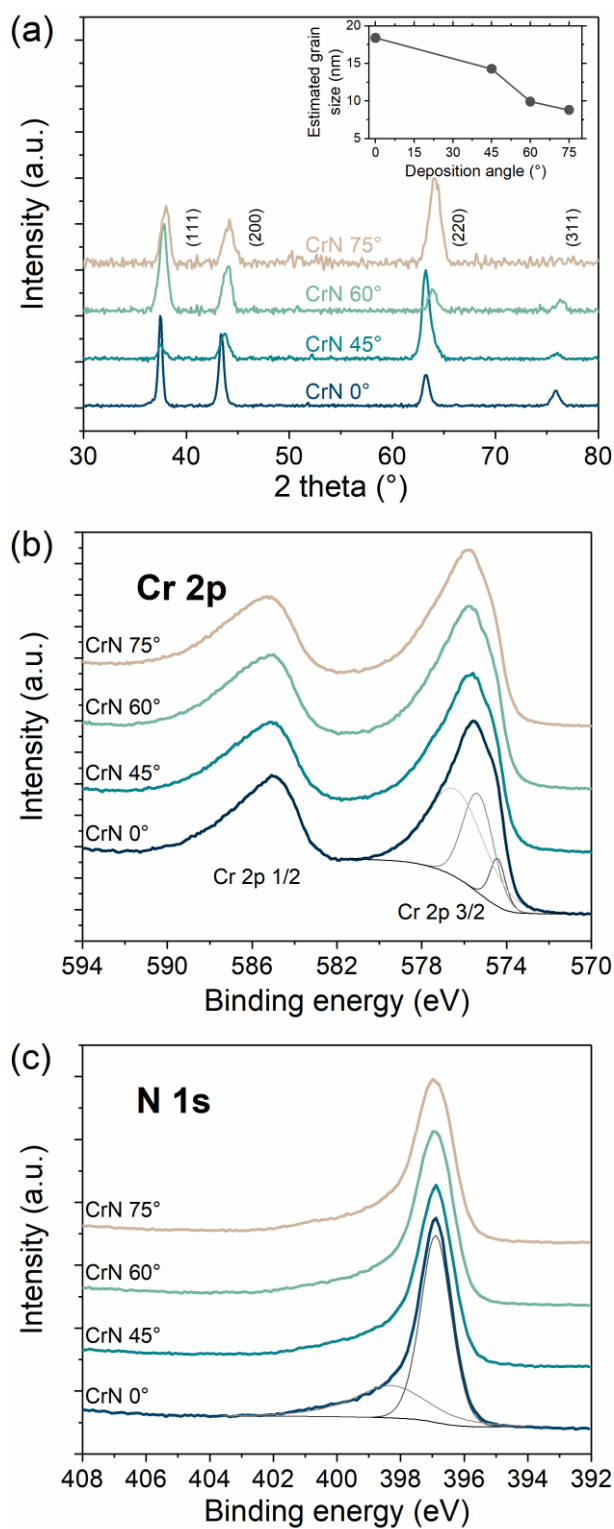


Fig.2. (a) XRD patterns, and XPS high-resolution spectra of (b) N 1s and (c) Cr 2p of CrN films.

1 The surface chemistry of the chromium nitride thin films has been investigated by XPS
2 measurements, on Cr 2p and N 1s core level spectra (Figure 2b and c). No significant
3 differences between samples are evidenced, which is expected, since neither the working
4 pressure nor the gas flux have been modified. The survey spectra (not shown here) reveal the
5 presence of oxygen, with higher content as the tilting angle increases. Cr 2p_{3/2} is fitted with
6 three contributions, centred at 574.6, 575.5 and 576.6 eV that can be assigned to CrN,
7 Cr(O,N) and Cr₂O₃, respectively [31]. Such surface oxidation is expected, as no sample
8 etching is done prior to the analysis. Nitride formation is attested on the N 1s core level
9 spectra (Figure 2c) with a major contribution at 396.9 eV in addition to oxynitride formation
10 as depicted from the contribution at 398.3 eV [31,32]. Since the specific capacitance of
11 electrochemical capacitors is influenced by both the surface chemistry and the surface area of
12 the active materials, one should consider that, in the case of our CrN electrodes, any
13 difference of the electrochemical behaviour will be only attributed to the effect of surface
14 area and structure, because the surface chemistry of all the CrN electrodes deposited at
15 different tilt angles is almost the same.
16
17
18
19
20
21
22
23
24
25
26
27
28
29
30
31
32
33
34
35
36
37
38
39

40 **3.2.2. Electrochemical properties**

41
42 The charge transfer and ion diffusion properties of the CrN thin film electrodes were
43 investigated by electrochemical impedance spectroscopy (EIS) measurements. Figure 3
44 shows the typical Nyquist and bode plots of CrN thin film electrodes (CrN0°, CrN45°,
45 CrN60° and CrN75°) recorded in 0.5 M H₂SO₄ aqueous solution at open circuit potential
46 (OCP).
47
48
49
50
51
52
53
54
55
56
57
58
59
60
61
62
63
64
65

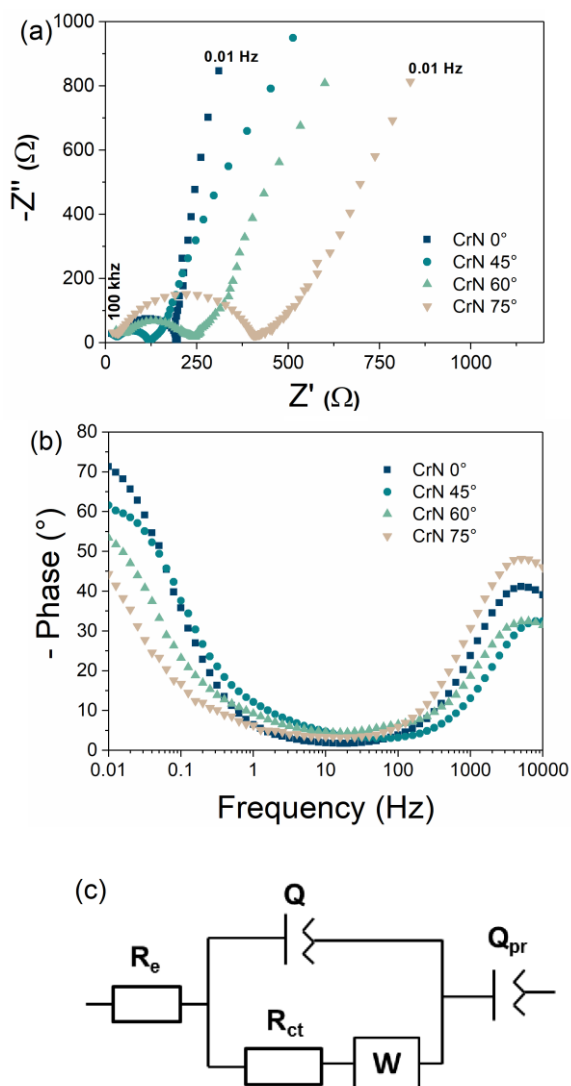


Fig.3. Analysis of EIS plots of the CrN film electrodes (CrN0°, CrN45°, CrN60° and CrN75°): (a) Nyquist plots, (b) Bode plots recorded in 0.5 M H₂SO₄ at OCP, and (c) the related equivalent circuit.

Figure 3 shows the comparison of EIS results for the different CrN film electrodes (CrN0°, CrN45°, CrN60° and CrN75°), with the Nyquist plots (Figure 3a), the Bode plots (Figure 3b), and (c) the Randles equivalent circuit (Figure 3c). Three domains can be identified for the EIS spectra as depicted in the Fig.3; at high frequencies region, a semicircle is observed which can be attributed to the surface properties and charge transfer resistance of the

1 material; the domain at mid frequencies region corresponds to straight line (except for
2 CrN0°) with a slope $< 45^\circ$ followed by straight line at higher phase angle. These features
3 indicate a non-perfect capacitive-like behavior. The slope of the straight line making an angle
4 lower than 45° in the mid-frequency region is due to the diffusion effect of ions at the
5 electrode–electrolyte interface and reflects the diffusive behaviour, including proton diffusion
6 in the electrolyte trapped in the porosity of the CrN film. These slopes are followed by a
7 straight line with a slope $> 45^\circ$ indicating the capacitive behaviour of the CrN films. These
8 results are in accordance with the literature on the electrochemical behavior of CrN in acidic
9 medium [18,33,34]. The intercept of the beginning of the semicircle with Z' axis is very close
10 for all the samples and it is related to the resistance of the 0.5M H₂SO₄ electrolyte (R_e).
11 Wider arcs or semi-circles mean greater resistance to charge transfer and a steeper slope
12 means a lower ion diffusion rate [35]. In the low frequency region, a vertical plot is observed,
13 suggesting a capacitive behavior of the CrN electrodes. The phase angles determined in the
14 Bode plot (Fig.3b) at low frequencies are $>45^\circ$ for all electrodes, which is lower than the
15 expected value for an ideal capacitor (90°). The Randles equivalent circuit of CrN electrodes
16 in Fig3.c presents three series networks, one of them related to the electrolyte, the second to
17 the film area, and the third to the pores. The electrolyte resistance is represented by resistor
18 R_e, the area occupied by CrN film is represented by a parallel R//Q network that refers to the
19 associated interfacial process (R_{ct}, C_{dl} and W), standing for the charge transfer resistance,
20 double layer capacitance and diffusion effect, respectively, in series with a Q_{pr} corresponding
21 to the pseudocapacitance of CrN electrodes. The Nyquist plot was fitted using the Randles
22 equivalent circuit and its parameter values were summarized in the Table 1. The resistance of
23 the electrolyte R_e was varied from 28 to 17 Ω which due to the difference in contact of the
24 back side of the electrodes. The charge transfer resistance (R_{ct}) value determined for CrN45°
25 electrode was 120 Ω, lower than that for CrN0°, CrN60° and CrN75° electrodes its values
26
27
28
29
30
31
32
33
34
35
36
37
38
39
40
41
42
43
44
45
46
47
48
49
50
51
52
53
54
55
56
57
58
59
60
61
62
63
64
65

were 204, 237, and 409 Ω , respectively. The results indicate that the CrN45° electrode is electrochemically more active than the other samples deposited at different grazing angles. This implies that the deposition angle has a drastic influence on the electrochemical behaviour of the CrN films. This can be explained by the morphology and the apparent porosity of the sample. The relative low charge transfer resistance (R_{ct}) values are helpful to provide good electrochemical performance [36].

Table 1. EIS equivalent circuit fitting parameter values of the CrN Electrodes in the electrolyte of 0.5M H₂SO₄.

	R_e (Ω)	Q (F)	R_{ct} (Ω)	W (S.sec ^{0.5})	B (sec ^{0.5})	Q_{pr} (S.sec ^{0.n})	n
0°	17.3	6.3×10^{-8}	204	3.6×10^{-3}	4.8×10^9	5.0×10^{-6}	0.8532
45°	18.1	7.7×10^{-3}	120	1.9×10^{-3}	2.4×10^5	5.1×10^{-6}	0.7833
60°	28.7	5.8×10^{-4}	237	5.9×10^{-3}	3.1×10^8	3.4×10^{-5}	0.5864
75°	19.8	6.3×10^{-7}	409	4.9×10^{-3}	2.4×10^9	9.6×10^{-7}	0.9443

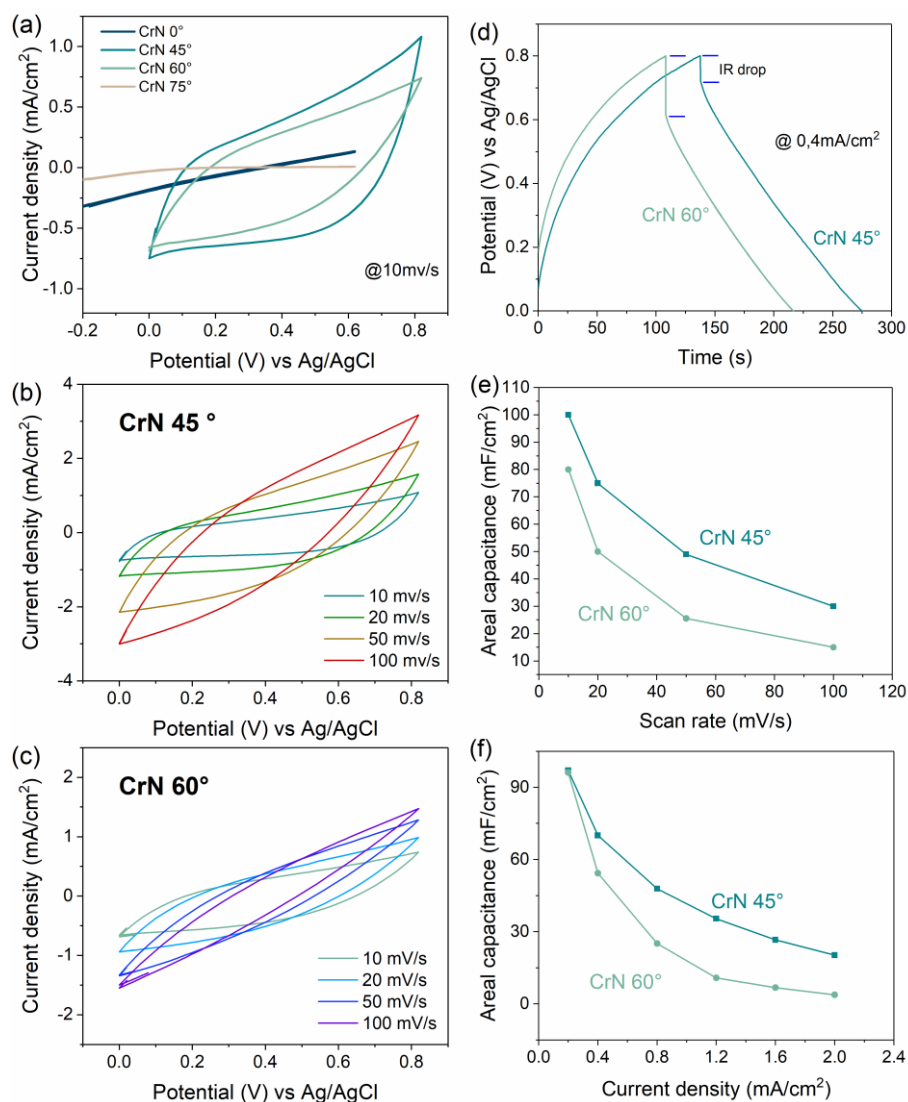


Fig. 4. (a) Comparison of cyclic voltammograms of CrN electrodes in 0.5M H₂SO₄ at a scan rate of 10 mV.s⁻¹, (b) cyclic voltammograms of CrN45° at different scan rates and (c) cyclic voltammograms of CrN60° at different scan rates, (d) comparison of GCD curves at 0.4 mA cm⁻² for CrN45° and CrN60° electrodes, (e) areal capacitance of CrN45° and CrN60° films versus scan rate, (f) areal capacitance of CrN45° and CrN60° films versus current density.

Figure 4a shows cycling voltammograms (CV) of the CrN (0-75°) electrodes at a scan rate of 10 mV.s⁻¹. The slight distortion of CrN45° and CrN60° CVs can be attributed to the electrical resistivity of CrN deposit. Indeed, the resistivity of the film increases from 5.5×10^{-2} , 1.2×10^{-1} ,

1
2
3
4
5
6
7
8
9
10
11
12
13
14
15
16
17
18
19
20
21
22
23
24
25
26
27
28
29
30
31
32
33
34
35
36
37
38
39
40
41
42
43
44
45
46
47
48
49
50
51
52
53
54
55
56
57
58
59
60
61
62
63
64
65

2.0×10^{-2} , and $6.9 \times 10^{-2} \Omega \cdot \text{cm}$ for CrN0°, CrN45°, CrN60° and CrN75°. The increase of the resistivity is attributed to the lower deposition rate as the deposition angle increase: the residual oxygen content is the same in the chamber, but due to a lower deposition rate, its content increases. In the case of CrN0° and CrN75°, the CVs do not show any capacitive behaviour even at low scan rate of $5 \text{ mV} \cdot \text{s}^{-1}$ (not shown here), and the current is very weak, thus indicating a poor double layer capacitance. This can be assigned to the dense structure of the CrN0° and CrN75° electrodes as observed by SEM and in agreement with EIS analyses. The effect of surface chemistry can be ruled out as already discussed in the XPS section. The CVs at different scan rates ($10\text{-}100 \text{ mV} \cdot \text{s}^{-1}$) of the CrN films, deposited at tilt angles of 45° and 60°, are presented in Figures 4b and 4c, respectively. At low scan rate, their both CVs exhibit small distortion, indicative of resistivity nature of the deposit (more portably due the increased oxygen amount in the films). However, at higher scan rates, the CrN45° and CrN60° electrodes display poor capacitance retention, which may be due to the porosity of the electrodes.

Galvanostatic charge-discharge curves at a current density of $0.4 \text{ mA} \cdot \text{cm}^{-2}$ are depicted in Figure 4d. It can be seen that the CrN45° and CrN60° electrodes display an IR drop of 0.088 V and 0.192 V respectively, suggesting a superior electrical conductivity of CrN45°, as well as more accessible porosity by the electrolyte. This is consistent with the CV and EIS results. Indeed, at the same scan rate, the CVs of CrN60° electrode are more distorted than those of CrN45° electrode.

The areal capacitance values were calculated from the charge-discharge curves at a current density of $0.400 \text{ mA} \cdot \text{cm}^{-2}$. The values are 70.0 and 54.2 $\text{mF} \cdot \text{cm}^{-2}$ for CrN45° and CrN60° electrodes, respectively. Such a difference cannot be due to the smaller thickness of CrN60° compared to CrN45°. Indeed, when the capacitance is normalized to the thickness, the volumetric capacitance of CrN 45° and CrN60° become 454.5 and 389.9 $\text{F} \cdot \text{cm}^{-3}$, respectively.

In Figures 4e and f are presented the variation of the areal capacitance versus scan rate and current density, respectively. It can be seen that the capacitance decreases with increasing the scan rate and current density, suggesting that parts of the surface are inaccessible at high scan rates and/or at fast charging-discharging rates. The difference of areal capacitance between the two electrodes can be attributed to the small differences in their thicknesses. It is noteworthy to mention that the capacitance values versus current density given in this work can be overestimated. This is because we used the slop method to estimate the capacitance versus the current densities, while this method is accurate only for ideally rectangular-shaped CV curves and triangular-shaped CD curves and which is not the case for our electrodes.

The capacity loss after 10,000 consecutive cycles at a scan rate of $100 \text{ mV}\cdot\text{s}^{-1}$ is only 5.5%, as shown in Figure 5, indicative of a fair long-term electrochemical stability [6–8], which is even higher than those of transition metal nitride materials [37]. Such a good electrochemical stability enables to envision the use of CrN electrodes in micro-supercapacitors [8]. The sudden drop in capacitance at the ~ 5000 cycle could be due to ON/OFF/ON room temperature change.

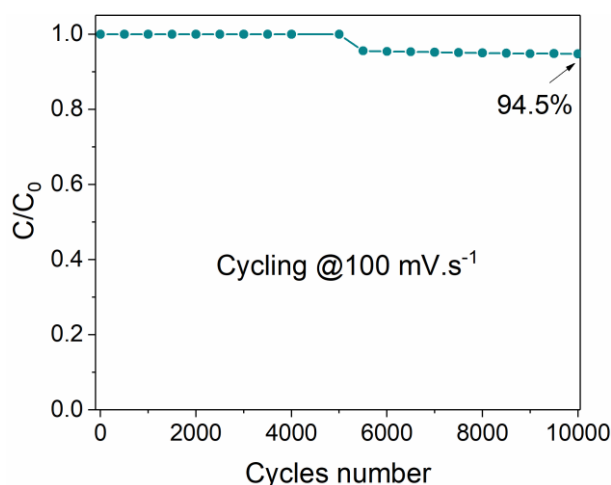


Fig.5. Cycling stability test of CrN_{45°} film in 0.5M H₂SO₄ at a scan rate of $100 \text{ mV}\cdot\text{s}^{-1}$.

1
2 From a practical point of view, the areal capacitance of $35.4 \text{ mF}\cdot\text{cm}^{-2}$ at a current density of
3 $1.2 \text{ mA}\cdot\text{cm}^{-2}$ for the CrN 45° electrode compares to 31.0 mF cm^{-2} at $1.0 \text{ mA}\cdot\text{cm}^{-2}$ for the
4 porous CrN electrodes recently reported in [19] and 2.5 fold higher than the best CrN
5 electrode deposited by sputtering ($13 \text{ mF}\cdot\text{cm}^{-2}$ at $1.0 \text{ mA}\cdot\text{cm}^{-2}$) recently reported in [18].
6
7 When compared to other transition metal nitrides, the areal capacitance of our CrN electrodes
8
9 is still much higher than for TiN electrodes ($27 \text{ mF}\cdot\text{cm}^{-2}$ at $1.0 \text{ mA}\cdot\text{cm}^{-2}$) [38], HfN electrode
10
11 ($6 \text{ mF}\cdot\text{cm}^{-2}$ at $1.0 \text{ mA}\cdot\text{cm}^{-2}$) [39], or GaN membrane (21 mF cm^{-2} at 0.1 mA cm^{-2}) [40].
12
13 Therefore, our CrN electrodes are competing quite well with the state of the art transition
14
15 metal nitride thin film electrodes, not only in the term of cycling stability but also in the term
16
17 of specific capacitance. A more detailed table is provided in the supplementary information
18
19 (Table S1) providing a comparison of our electrodes with other materials.
20
21
22
23
24
25
26
27
28
29

30 **3.2. Integration of CrN thin film electrode in a planar symmetrical micro-** 31 **supercapacitor**

32
33
34
35 A symmetrical microsupercapacitor (MSC) was fabricated using CrN thin films (CrN 45° or
36
37 CrN 60°) as electrodes, as depicted in Figure 6a-b. More details for MSC fabrication are
38
39 given in the supplementary information. The technological process used for micro-device
40
41 fabrication allows us to perform the collective fabrication of MSCs at a wafer scale. CrN 60°
42
43 was chosen in this study to be integrated on the micro-device. As the volumetric capacitance
44
45 is close to each other for both orientations, we choose the more tilted sample, namely CrN
46
47 60° . In addition, due to the size of the device and in order to avoid deposition on the current
48
49 collector side of the device, orientation of 60° was chosen as safe angle in order to deposit
50
51 the CrN on the device. More than 95% of the 30 fabricated MSCs did not exhibit any short-
52
53 circuit between the two electrodes, indicating the high reproducibility of the technological
54
55
56
57
58
59
60
61
62
63
64
65

process. Furthermore, the electrodes are deposited without intentional heating of the silicon substrate. Therefore, our complete process is compatible with semiconductor technology.

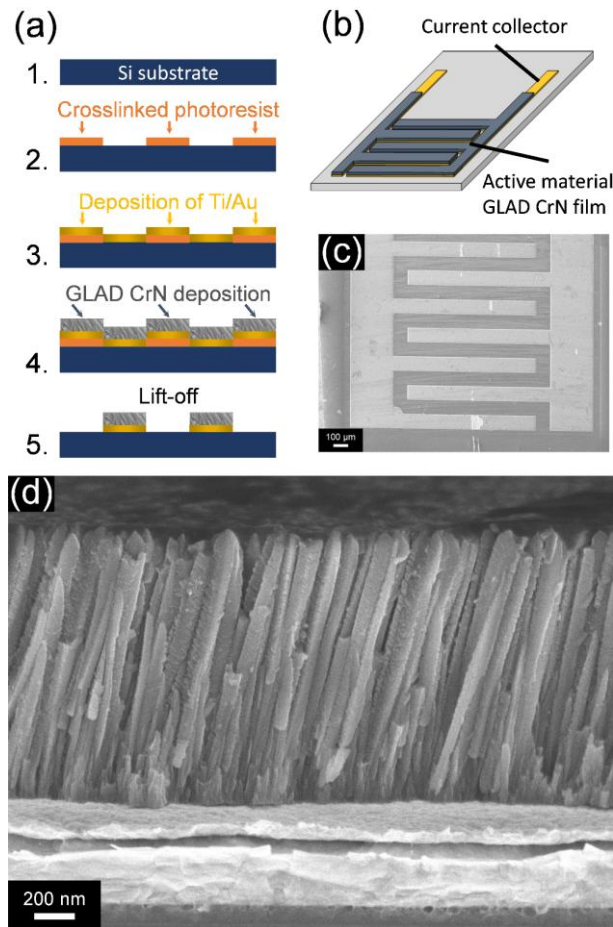


Fig.6. Micro-supercapacitor fabrication and design. (a) Schematic illustration of the fabrication process using the lift-off process of the active material (not to scale). Schematic (b) and optical image (c) of the micro-device. (d) Cross-section of the electrode observed with scanning electron microscopy.

Figure 6c illustrates the geometrical parameters of the unit cell. A 100 μm wide spacing was used to isolate the interdigitated electrodes (2 mm long/1.7 mm wide). The SEM cross-section of the CrN coated MSCs is reported in Figure 6d, with a similar morphology with previous coatings.

CVs were recorded at a scan rate from 0.01 to 10 V.s⁻¹ to test the rate capability of the MSCs.

Indeed, the integration of CrN on chip MSCs allows decreasing the series resistance thus improving the power density of the microsystem [41].

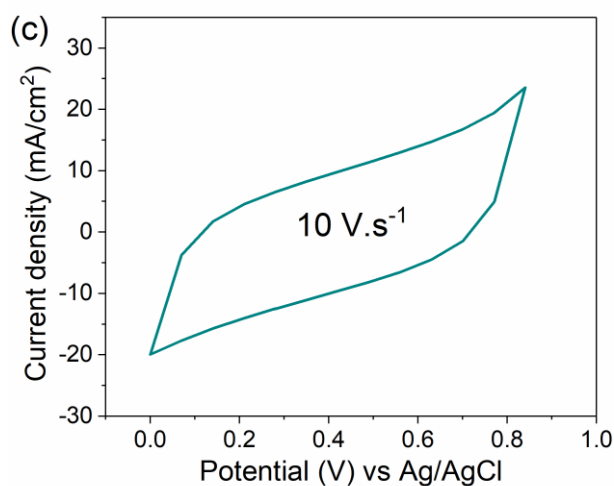
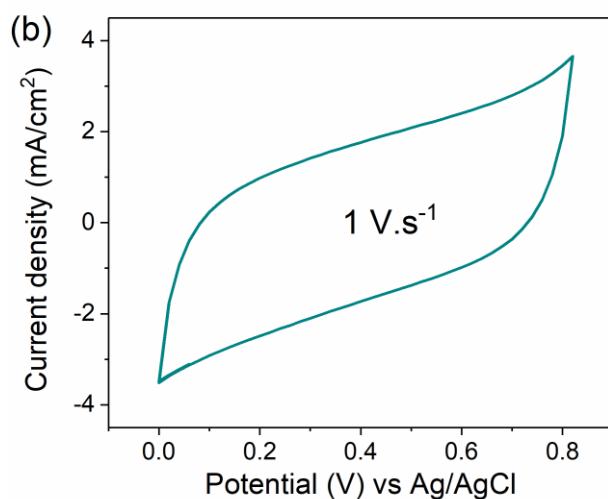
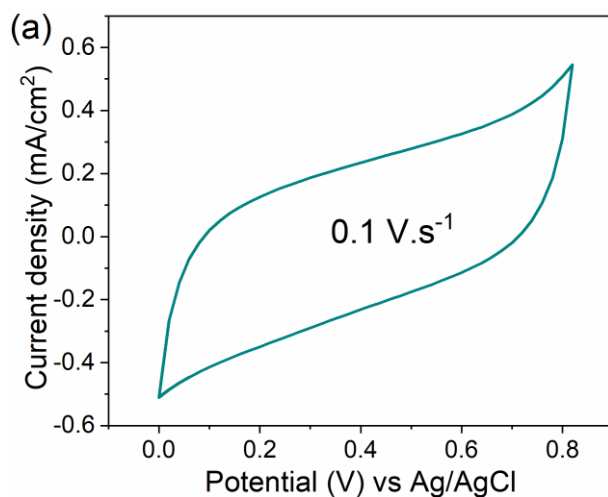


Fig.7. CVs obtained at scan rates of (a) 0.1, (b) 1 and (c) 10 V.s⁻¹ for CrN 60° based micro-supercapacitor device.

The shape of the Nyquist plots (Figure S3) clearly confirms no short circuit between the electrodes, thus validating again the technological process. Electrochemical impedance spectroscopy was used to investigate the CrN micro-supercapacitor device. The electrolyte resistance between the two CrN electrodes is 13.0 Ω. The charge transfer resistance values (R_{ct}) determined for the symmetric micro-supercapacitor is 36.8 Ω. The galvanostatic charge-discharge curves at different current densities of the MSCs in 0.5 M H₂SO₄ are displayed in Figure 8a. The areal capacitance measured at the lower current density (0.05 mA cm⁻²) is 10.3 mF cm⁻². Since the surface area of a single electrode is less than 1/3 of the total surface of the micro-device, this capacitance value is in good agreement with the previous findings from the study of single electrodes. Indeed, a capacitance of 10.3 mF cm⁻² for the MSC is 25% of that of the corresponding thin film (≈ 35.4 mF cm⁻² per electrode), in agreement with surface ratio.

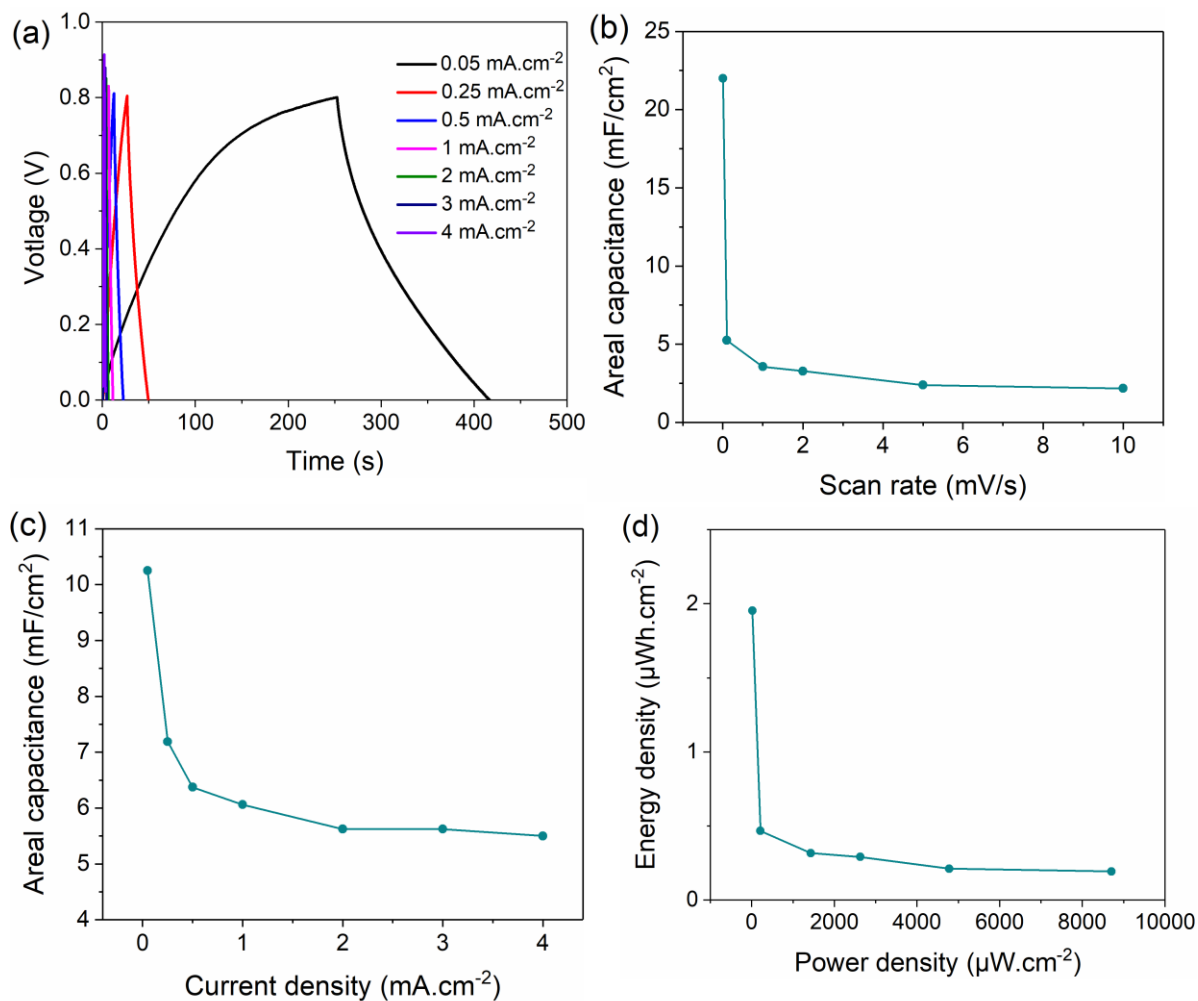


Fig.8. (a) GCD curves of CrN 60° based micro-supercapacitor at different current densities, (b) its areal capacitance versus scan rate and (c) its areal capacitance versus current density, (d) Ragone plot.

It can be seen that at a current density of 0.05 mA.cm⁻², the CrN60° based MSC displays an IR drop of 0.088 V versus 0.192 V for CrN60° thin film electrode (Fig.4d), indicating less resistance in series for the MSC. Which is also the reason why the integrated CrN60° can be cycled at higher scan rate compared to the same deposit tested in the three electrodes configuration. In Figure 8b and c are presented the variation of the areal capacitance with scan rate and current density, respectively. The values of areal capacitances experience a drastic drop upon increasing the scan rate from 2 to 100 mV.s⁻¹ (from 21.0 to 5.5 mF.cm⁻²), whereas a relatively high capacitance level is retained over scan rates in the wide range of

0.1–10 V.s⁻¹ (from 5.5 to 2.2 mF.cm⁻²). The decrease in capacitance with scan rate increase from 2 to 100 mV.s⁻¹ occurs not only due to the limited ion diffusion in porous electrodes, but also to the limitation from charge transfer rate for pseudo-capacitive electrodes. The same phenomenon happens for current densities in the range of 0.05-1 mA.cm⁻² and 1- 4 mA.cm⁻². For the former current range, the areal capacitance is stable around 6.0 and 5.5 mF. cm⁻², while it drops from 10.3 to 6.0 mF. cm⁻² within the of 0.05- 1 mA.cm⁻² current range.

Considering the thickness of the coating, the volumetric capacitance is stable around 40-45 F.cm⁻³. Although the mass of the device is not really meaningful, as the area is more important than its mass [8], the mass loading can be roughly estimated from Rutherford Backscattering Spectroscopy (RBS) measurements. The complete study of the density variation as a function of the deposition angle is beyond the scope of this paper (but will be studied in a forthcoming work), but preliminary RBS measurements have been performed on CrN thin film deposited at a tilt of 60°, giving an RBS density is of ≈4.5g.cm⁻³. Considering the volume of the device, and the coating thickness, the mass loading is around 2×10⁻² mg.

The areal capacitance of the symmetric CrN/CrN based MSC is higher than the silicon chip CDC MSCs (1.5 mF.cm⁻² at 100 mV.s⁻¹) [42], and comparable to the PS–TiN in-chip device (5 mF.cm⁻²) [37], photoresist derived carbon (3.2 mF cm⁻² at 0.5 mA.cm⁻²) [43], or asymmetric flexible MXene- reduced graphene oxide (2.4 mF cm⁻² at 2 mV.s⁻¹) [44]

The maximum surface power density of the 1.3μm thick CrN60°/CrN60° symmetrical MSC was 8.7 mW.cm⁻² at an energy density of 0.2 μWh.cm⁻². This energy can be increased up to 2 μWh.cm⁻² while decreasing the power density to 20 μW.cm⁻². Although the energy density is impeded by the limited cell voltage (0.8 V) due to the use of symmetrical device in acidic electrolyte, the high values of power density depict the optimum geometry of our electrodes and microdevices.

4. Conclusion

In this work, GLAD deposition technique was used to deposit CrN films for use as electrodes for electrochemical capacitors. The films deposited at 0° and 75° are electrochemically inactive for charge storage, more probably due to inappropriate morphologies (too dense at 0° and inaccessible columns closed on the top at 75°), while films deposited at 45 and 60° exhibit a columnar morphology, with open voids that allow access for ion diffusion onto the electroactive interface, resulting in electrode with high specific capacitance (35.4 mF cm⁻² at a current density of 1.2 mA.cm⁻²) and long cycling life (94.5% of retention after 10.000 cycles). In addition, our symmetric on chip micro-supercapacitor based on porous CrN60° demonstrate a maximum energy density of 2 μWh.cm⁻² (15.3 mWh.cm⁻³) at a power density of 20 μW.cm⁻² (0.15 W.cm⁻³). Moreover, power densities can be increased up to 8.7 mW.cm⁻². Although preliminary, these first results open the way for the fabrication of on-chip CrN based microsupercapacitors using GLAD deposition technique. Further work should aim at enlarging the cell voltage of the microdevice by coupling CrN as positive electrode with another negative electrode such as vanadium nitride.

Acknowledgement

The Synthesis Irradiation and Analysis of Materials (SIAM), PC² and MORPH-IM platforms of UNamur are acknowledged for XPS, XRD and SEM measurements.

References

- 1
2
3
4 [1] K. Ait Aissa, A. Achour, J. Camus, L. Le Brizoual, P.-Y. Jouan, M.-A. Djouadi,
5
6 Comparison of the structural properties and residual stress of AlN films deposited by dc
7
8 magnetron sputtering and high power impulse magnetron sputtering at different working
9
10 pressures, *Thin Solid Films*. 550 (2014) 264–267. doi:10.1016/j.tsf.2013.11.073.
11
12
13
14 [2] E. Haye, J.L. Colaux, P. Moskovkin, J.-J. Pireaux, S. Lucas, Wide range investigation
15
16 of duty cycle and frequency effects on bipolar magnetron sputtering of chromium nitride,
17
18 *Surf. Coat. Technol.* 350 (2018) 84–94. doi:10.1016/j.surfcoat.2018.07.009.
19
20
21
22 [3] L. Bait, L. Azzouz, N. Madaoui, N. Saoula, Influence of substrate bias voltage on the
23
24 properties of TiO₂ deposited by radio-frequency magnetron sputtering on 304L for
25
26 biomaterials applications, *Appl. Surf. Sci.* 395 (2017) 72–77.
27
28 doi:10.1016/j.apsusc.2016.07.101.
29
30
31
32 [4] Z. Ben Cheikh, F. El Kamel, O. Gallot-Lavallée, M.A. Soussou, S. Vizireanu, A.
33
34 Achour, K. Khirouni, Hydrogen doped BaTiO₃ films as solid-state electrolyte for micro-
35
36 supercapacitor applications, *J. Alloys Compd.* 721 (2017) 276–284.
37
38 doi:10.1016/j.jallcom.2017.06.019.
39
40
41
42 [5] J.F.M. Oudenhoven, Loïc. Baggetto, P.H.L. Notten, All-Solid-State Lithium-Ion
43
44 Microbatteries: A Review of Various Three-Dimensional Concepts, *Advanced Energy*
45
46 *Materials*. 1 (2011) 10–33. doi:10.1002/aenm.201000002.
47
48
49
50
51 [6] J. Freixas, E. Eustache, P. Roussel, C. Brillard, D. Deresmes, N. Nuns, N. Rolland, T.
52
53 Brousse, C. Lethien, Sputtered Titanium Nitride: A Bifunctional Material for Li-Ion
54
55 Microbatteries, *J. Electrochem. Soc.* 162 (2015) A493–A500. doi:10.1149/2.0051504jes.
56
57
58
59
60
61
62
63
64
65

- 1
2
3
4
5
6
7
8
9
10
11
12
13
14
15
16
17
18
19
20
21
22
23
24
25
26
27
28
29
30
31
32
33
34
35
36
37
38
39
40
41
42
43
44
45
46
47
48
49
50
51
52
53
54
55
56
57
58
59
60
61
62
63
64
65
- [7] P. Simon, Y. Gogotsi, Materials for electrochemical capacitors, *Nature Materials*. 7 (2008) 845–854. doi:10.1038/nmat2297.
- [8] N.A. Kyeremateng, T. Brousse, D. Pech, Microsupercapacitors as miniaturized energy-storage components for on-chip electronics, *Nature Nanotechnology*. 12 (2017) 7–15. doi:10.1038/nnano.2016.196.
- [9] P. Huang, C. Lethien, S. Pinaud, K. Brousse, R. Laloo, V. Turq, M. Respaud, A. Demortière, B. Daffos, P.L. Taberna, B. Chaudret, Y. Gogotsi, P. Simon, On-chip and freestanding elastic carbon films for micro-supercapacitors, *Science*. 351 (2016) 691–695. doi:10.1126/science.aad3345.
- [10] A. Guerra, A. Achour, S. Vizireanu, G. Dinescu, S. Messaci, T. Hadjersi, R. Boukherroub, Y. Coffinier, J.-J. Pireaux, ZnO/Carbon nanowalls shell/core nanostructures as electrodes for supercapacitors, *Applied Surface Science*. 481 (2019) 926–932. doi:10.1016/j.apsusc.2019.03.204.
- [11] M.-J. Lee, J.S. Kim, S.H. Choi, J.J. Lee, S.H. Kim, S.H. Jee, Y.S. Yoon, Characteristics of thin film supercapacitor with ruthenium oxide electrode and Ta₂O_{5+x} solid oxide thin film electrolyte, *J Electroceram*. 17 (2006) 639–643. doi:10.1007/s10832-006-7777-z.
- [12] A. Kumar, A. Sanger, A. Kumar, Y. Kumar, R. Chandra, Sputtered Synthesis of MnO₂ Nanorods as Binder Free Electrode for High Performance Symmetric Supercapacitors, *Electrochim. Acta*. 222 (2016) 1761–1769. doi:10.1016/j.electacta.2016.10.161.
- [13] A. Achour, R.L. Porto, M.-A. Soussou, M. Islam, M. Boujtita, K.A. Aissa, L. Le Brizoual, A. Djouadi, T. Brousse, Titanium nitride films for micro-supercapacitors: Effect of surface chemistry and film morphology on the capacitance, *Journal of Power Sources*. 300 (2015) 525–532. doi:10.1016/j.jpowsour.2015.09.012.

- 1
2
3
4
5
6
7
8
9
10
11
12
13
14
15
16
17
18
19
20
21
22
23
24
25
26
27
28
29
30
31
32
33
34
35
36
37
38
39
40
41
42
43
44
45
46
47
48
49
50
51
52
53
54
55
56
57
58
59
60
61
62
63
64
65
- [14] A. Achour, M. Chaker, H. Achour, A. Arman, M. Islam, M. Mardani, M. Boujtita, L. Le Brizoual, M.A. Djouadi, T. Brousse, Role of nitrogen doping at the surface of titanium nitride thin films towards capacitive charge storage enhancement, *Journal of Power Sources*. 359 (2017) 349–354. doi:10.1016/j.jpowsour.2017.05.074.
- [15] A. Achour, R. Lucio-Porto, S. Solaymani, M. Islam, I. Ahmad, T. Brousse, Reactive sputtering of vanadium nitride thin films as pseudo-capacitor electrodes for high areal capacitance and cyclic stability, *J Mater Sci: Mater Electron*. 29 (2018) 13125–13131. doi:10.1007/s10854-018-9435-z.
- [16] A. Achour, R. Lucio-Porto, M. Chaker, A. Arman, A. Ahmadpourian, M.A. Soussou, M. Boujtita, L. Le Brizoual, M.A. Djouadi, T. Brousse, Titanium vanadium nitride electrode for micro-supercapacitors, *Electrochemistry Communications*. 77 (2017) 40–43. doi:10.1016/j.elecom.2017.02.011.
- [17] S. Bouhtiyaa, R. Lucio Porto, B. Laïk, P. Boulet, F. Capon, J.P. Pereira-Ramos, T. Brousse, J.F. Pierson, Application of sputtered ruthenium nitride thin films as electrode material for energy-storage devices, *Scripta Materialia*. 68 (2013) 659–662. doi:10.1016/j.scriptamat.2013.01.030.
- [18] B. Wei, H. Liang, D. Zhang, Z. Wu, Z. Qi, Z. Wang, CrN thin films prepared by reactive DC magnetron sputtering for symmetric supercapacitors, *J. Mater. Chem. A*. 5 (2017) 2844–2851. doi:10.1039/C6TA09985H.
- [19] B. Wei, G. Mei, H. Liang, Z. Qi, D. Zhang, H. Shen, Z. Wang, Porous CrN thin films by selectively etching CrCuN for symmetric supercapacitors, *Journal of Power Sources*. 385 (2018) 39–44. doi:10.1016/j.jpowsour.2018.03.023.
- [20] K. Robert, C. Douard, A. Demortière, F. Blanchard, P. Roussel, T. Brousse, C. Lethien, On Chip Interdigitated Micro-Supercapacitors Based on Sputtered Bifunctional

1 Vanadium Nitride Thin Films with Finely Tuned Inter- and Intracolumnar Porosities,
2 Advanced Materials Technologies. 3 (2018) 1800036. doi:10.1002/admt.201800036.
3
4

5 [21] A. Besnard, N. Martin, C. Millot, J. Gavaille, R. Salut, Effect of sputtering pressure
6 on some properties of chromium thin films obliquely deposited, IOP Conf. Ser.: Mater. Sci.
7 Eng. 12 (2010) 012015. doi:10.1088/1757-899X/12/1/012015.
8
9

10 [22] B. Bouaouina, C. Mastail, A. Besnard, R. Mareus, F. Nita, A. Michel, G. Abadias,
11 Nanocolumnar TiN thin film growth by oblique angle sputter-deposition: Experiments vs.
12 simulations, Materials & Design. 160 (2018) 338–349. doi:10.1016/j.matdes.2018.09.023.
13
14
15

16 [23] X. Xu, M. Arab Pour Yazdi, J.-B. Sanchez, A. Billard, F. Berger, N. Martin,
17 Exploiting the dodecane and ozone sensing capabilities of nanostructured tungsten oxide
18 films, Sensors and Actuators B: Chemical. 266 (2018) 773–783.
19 doi:10.1016/j.snb.2018.03.190.
20
21

22 [24] G. Greczynski, J. Jensen, J. Böhlmark, L. Hultman, Microstructure control of CrNx
23 films during high power impulse magnetron sputtering, Surf. Coat. Technol. 205 (2010) 118–
24 130. doi:10.1016/j.surfcoat.2010.06.016.
25
26
27

28 [25] J. Dervaux, P.-A. Cormier, S. Konstantinidis, P. Moskovkin, S. Lucas, R. Snyders,
29 Nanostructured Ti thin films by combining GLAD and magnetron sputtering: a joint
30 experimental and modeling study, 22nd International Symposium on Plasma Chemistry.
31 (2015) 4.
32
33
34

35 [26] J. Dervaux, P.-A. Cormier, S. Konstantinidis, R. Di Ciuccio, O. Coulembier, P.
36 Dubois, R. Snyders, Deposition of porous titanium oxide thin films as anode material for dye
37 sensitized solar cells, Vacuum. 114 (2015) 213–220. doi:10.1016/j.vacuum.2014.10.016.
38
39
40
41
42
43
44
45
46
47
48
49
50
51
52
53
54
55
56
57
58
59
60
61
62
63
64
65

- 1
2
3
4
5
6
7
8
9
10
11
12
13
14
15
16
17
18
19
20
21
22
23
24
25
26
27
28
29
30
31
32
33
34
35
36
37
38
39
40
41
42
43
44
45
46
47
48
49
50
51
52
53
54
55
56
57
58
59
60
61
62
63
64
65
- [27] J. Lintymer, J. Gavaille, N. Martin, J. Takadoum, Glancing angle deposition to modify microstructure and properties of sputter deposited chromium thin films, *Surf. Coat. Technol.* 174–175 (2003) 316–323. doi:10.1016/S0257-8972(03)00413-4.
- [28] A. Barranco, A. Borrás, A.R. González-Elipé, A. Palmero, Perspectives on oblique angle deposition of thin films: From fundamentals to devices, *Progress in Materials Science.* 76 (2016) 59–153. doi:10.1016/j.pmatsci.2015.06.003.
- [29] A. Trenczek-Zajac, M. Radecka, K. Zakrzewska, A. Brudnik, E. Kusior, S. Bourgeois, M.C.M. de Lucas, L. Imhoff, Structural and electrical properties of magnetron sputtered Ti(ON) thin films: The case of TiN doped in situ with oxygen, *Journal of Power Sources.* 194 (2009) 93–103. doi:10.1016/j.jpowsour.2008.12.112.
- [30] N.K. Ponon, D.J.R. Appleby, E. Arac, P.J. King, S. Ganti, K.S.K. Kwa, A. O'Neill, Effect of deposition conditions and post deposition anneal on reactively sputtered titanium nitride thin films, *Thin Solid Films.* 578 (2015) 31–37. doi:10.1016/j.tsf.2015.02.009.
- [31] I. Milošev, H.-H. Strehblow, B. Navinšek, Comparison of TiN, ZrN and CrN hard nitride coatings: Electrochemical and thermal oxidation, *Thin Solid Films.* 303 (1997) 246–254. doi:10.1016/S0040-6090(97)00069-2.
- [32] H.C. Barshilia, N. Selvakumar, B. Deepthi, K.S. Rajam, A comparative study of reactive direct current magnetron sputtered CrAlN and CrN coatings, *Surf. Coat. Technol.* 201 (2006) 2193–2201. doi:10.1016/j.surfcoat.2006.03.037.
- [33] B. Das, M. Behm, G. Lindbergh, M.V. Reddy, B.V.R. Chowdari, High performance metal nitrides, MN (M=Cr, Co) nanoparticles for non-aqueous hybrid supercapacitors, *Advanced Powder Technology.* 26 (2015) 783–788. doi:10.1016/j.appt.2015.02.001.

- 1
2
3
4
5
6
7
8
9
10
11
12
13
14
15
16
17
18
19
20
21
22
23
24
25
26
27
28
29
30
31
32
33
34
35
36
37
38
39
40
41
42
43
44
45
46
47
48
49
50
51
52
53
54
55
56
57
58
59
60
61
62
63
64
65
- [34] Y. Wu, F. Ran, Vanadium nitride quantum dot/nitrogen-doped microporous carbon nanofibers electrode for high-performance supercapacitors, *Journal of Power Sources*. 344 (2017) 1–10. doi:10.1016/j.jpowsour.2017.01.095.
- [35] P.R. Jadhav, M.P. Suryawanshi, D.S. Dalavi, D.S. Patil, E.A. Jo, S.S. Kolekar, A.A. Wali, M.M. Karanjkar, J.-Hyeok. Kim, P.S. Patil, Design and electro-synthesis of 3-D nanofibers of MnO₂ thin films and their application in high performance supercapacitor, *Electrochim. Acta*. 176 (2015) 523–532. doi:10.1016/j.electacta.2015.07.002.
- [36] H. Shen, B. Wei, D. Zhang, Z. Qi, Z. Wang, Magnetron sputtered NbN thin film electrodes for supercapacitors, *Materials Letters*. 229 (2018) 17–20. doi:10.1016/j.matlet.2018.06.052.
- [37] K. Grigoras, J. Keskinen, L. Grönberg, E. Yli-Rantala, S. Laakso, H. Välimäki, P. Kauranen, J. Ahopelto, M. Prunnila, Conformal titanium nitride in a porous silicon matrix: A nanomaterial for in-chip supercapacitors, *Nano Energy*. 26 (2016) 340–345. doi:10.1016/j.nanoen.2016.04.029.
- [38] B. Wei, H. Liang, D. Zhang, Z. Qi, H. Shen, Z. Wang, Magnetron sputtered TiN thin films toward enhanced performance supercapacitor electrodes, *Materials for Renewable and Sustainable Energy*. 7 (2018). doi:10.1007/s40243-018-0117-9.
- [39] Z. Gao, Z. Wu, S. Zhao, T. Zhang, Q. Wang, Enhanced capacitive property of HfN film electrode by plasma etching for supercapacitors, *Mater. Lett.* 235 (2019) 148–152. doi:10.1016/j.matlet.2018.10.032.
- [40] L. Zhang, S. Wang, Y. Shao, Y. Wu, C. Sun, Q. Huo, B. Zhang, H. Hu, X. Hao, One-step fabrication of porous GaN crystal membrane and its application in energy storage, *Scientific Reports*. 7 (2017). doi:10.1038/srep44063.

- 1
2
3
4
5
6
7
8
9
10
11
12
13
14
15
16
17
18
19
20
21
22
23
24
25
26
27
28
29
30
31
32
33
34
35
36
37
38
39
40
41
42
43
44
45
46
47
48
49
50
51
52
53
54
55
56
57
58
59
60
61
62
63
64
65
- [41] D. Pech, M. Brunet, T.M. Dinh, K. Armstrong, J. Gaudet, D. Guay, Influence of the configuration in planar interdigitated electrochemical micro-capacitors, *Journal of Power Sources*. 230 (2013) 230–235. doi:10.1016/j.jpowsour.2012.12.039.
- [42] P. Huang, M. Heon, D. Pech, M. Brunet, P.-L. Taberna, Y. Gogotsi, S. Lofland, J.D. Hettinger, P. Simon, Micro-supercapacitors from carbide derived carbon (CDC) films on silicon chips, *Journal of Power Sources*. 225 (2013) 240–244. doi:10.1016/j.jpowsour.2012.10.020.
- [43] B. Hsia, M.S. Kim, M. Vincent, C. Carraro, R. Maboudian, Photoresist-derived porous carbon for on-chip micro-supercapacitors, *Carbon*. 57 (2013) 395–400. doi:10.1016/j.carbon.2013.01.089.
- [44] C. Couly, M. Alhabeab, K.L. Van Aken, N. Kurra, L. Gomes, A.M. Navarro-Suárez, B. Anasori, H.N. Alshareef, Y. Gogotsi, Asymmetric Flexible MXene-Reduced Graphene Oxide Micro-Supercapacitor, *Advanced Electronic Materials*. 4 (2018) 1700339. doi:10.1002/aelm.201700339.

Supplementary Materials

[Click here to download Supplementary Materials: REVISED-Supplementary-information.docx](#)